Instability of Electrically Driven Polymer Liquid Jets

Minhyung Lee*, Seung Baik Kang, Joo Hyuk Park
Department of Mechanical Engineering, Sejong University,
98 Kunja-Dong, KwangJin-Gu, Seoul 143-747, Korea

Polymer nanofibers can be generated by a electrospinning process. The process involves electrically charged jet of polymer solutions evolving from a droplet. The jet stretches in vertical direction due to the difference between charged particle and constant current located at the collector, while the Coulomb and viscoelastic forces start to contribute to radial and azimuthal (torsional) stretching. In this paper, the unstable dynamics of the liquid polymer jet is examined experimentally and theoretically. A complex viscoelastic rheological model has been adopted to analyze the behavior of a charged liquid jet. The model includes complex phenomena of stress relaxation of the liquid jet resulting from the competing force components. The experimental data of the jet paths captured by high-speed videocamera also confirm the similar behavior with the predictions.

Key Words : Electrospinning, Liquid Jet, Voscoelastic Liquid

1. Introduction

A number of processing techniques such as drawing, template synthesis, phase separation and electrospinning have been used to produce polymer nanofibers in recent years. Among them, electrospinning has been emerged as a cost effective and reliable method to produce nanofibers of diameter ranging from 3 nm to 1 μm. Due to high area-volume ratio, which is about 100 times larger than that of conventional microfiber, the practical applications of nanofibers are found in various medical and industrial fields such as wound dressings, drug delivery and reinforced composite. The technique takes advantage of Coulomb force between charged ions. The charged ions are confined in and are carried by a viscoelastic fluid. Unlike a Newtonian fluid, the viscoelastic force exhibits solid-like reponse as well as fluid-like reponse under the deformation by the repulsive force between charges.

The fluid contains electrical charges, which are excess charges. The (excess) charge denotes the difference in the number of positive and negative ions which are assumed to be evenly distributed in the fluid domain. In the presence of an external electrical field, positive and negative ions tend to migrate toward opposite directions. The negative (positive) ions are attracted toward the positive (negative) electrode. The charge mobility in solid is infinitely fast while that in a moving fluid is not as fast. In general, the conductivity of liquid can be enhanced by increasing ions per unit volume. However, the excess charge cannot change.

The work of thin liquid jet in electric field dates back to the work of Rayleigh (1882). The electrospinning process was first patented by Formhals and he succeeded to make fine polymer fibers (1934). Acrylic micro fiber was then produced in range from 0.05 to 1.1 microns by Baumgarten (1971). Other types of polymeric liquids were adopted to generate micro-thin fibers such as polyethelene, polypropylene (Larrondo and Manley 1981), polyethelene oxide (Doshi and Reneker 1995), polyamid (Dersch et al.,

* Corresponding Author,
E-mail : mlee@sejong.ac.kr
TEL : +82-2-3408-3282; **FAX** : +82-2-3408-3333
Department of Mechanical Engineering, Sejong University, 98 Kunja-Dong, KwangJin-Gu, Seoul 143-747, Korea. (Manuscript **Received** May 14, 2005; **Revised** January 26, 2006)

2003), polyvinylacetate (Viswanathamiruthi et al., 2003) and polyurethane (Pedicini and Farris 2003). Reneker and Chun (1996) suggest that electrospinning provides a straightforward and practical way to produce polymer fibers with diameters ranging from 40–2000 nm. The use of atomic force microscope (AFM) is found to be beneficial in finding a highly ordered surface pattern of electrospinning process. The experimental approaches are commonly used due to nano-scale phenomena. Thus, little has been devoted to the theoretical work of nanofiber system of realistic physical system.

The theoretical work associated with the electrospinning process dates back to the work of Taylor. The introduction of Taylor's cone greatly helps to identify unstable wave-like propagation of thin liquid jet (Taylor 1964). Taylor's theorem suggests the critical voltage at which the strongest instability develops. More recently, the minimum spraying potential was calculated for a suspended, hemisphere, conducting drop in air (Horning and Hendricks 1979). The rate of spinning and electric field strength was also estimated by measuring the length of PE fiber (Larrondo and Manley 1981). Fang and Reneker (1997) revealed a relationship between the strength of electric field, surface tension, air permeability and capillary radius. More recently, Reneker et al.(2000) identified the source of bending instability with a mathematical model. Shin et al.(2001) also investigated the stability of electrospinning jets using the method based on asymptotic expansion for the equation of electro-hydrodynamics.

In current research, we performed some experiments using a high-speed camera (CCD) to capture the evolution of a liquid polymer jet. A theoretical approach is then taken to represent the experimental data, such as the radial stretching and axial elongation in nanofiber. Since one of the most interesting characteristics arising in a viscoelastic fluid is stress relaxation, which determines the time when the stress relaxation occurs, we use a novel viscoelastic fluid model to describe the bending instability of the liquid jet. The model effectively accounts for the memory effect of polymeric liquid, which balances out with the repulsive Coulomb force. The equation of motion is presented in the three-dimensional frame of reference. The theoretical predictions are compared with the experimental data.

2. Experiments

Figure 1 shows the schematic view of current experimental apparatus. Since a difference in electrical potential is applied between the droplet and the collector, polymeric liquid emerges from a pendant drop and approaches to collector at a distance h from the pendant. A small syringe was used to inject a fluid droplet in the field. Once the force due to the electrical charge overcomes the surface tension effect near the nozzle exit, the droplet forms a fiber, which moves toward the collector. Then the fluid undergoes axial and lateral deformation in the presence of the Coulomb force (repulsion) and electric field from the collector (attraction).

The experiment was performed at room temperature. In order to capture the liquid jet without causing any disturbance to the electric field, a lens and a high-speed CCD camera were located 30 cm away from the nozzle exit. The camera is equipped with 24~70 mm, f 2.8 zoom lens and takes shots at every 0.5 ms (2000 frame/second). The source of light is 1000W halogen lamp. A

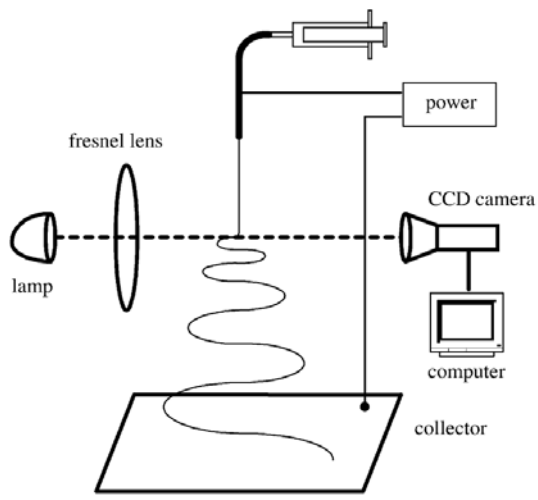

Fig. 1 Schematic view of experimental apparatus for the polymer liquid jets in electrospinning

frensel condenser lens of 30 cm diameter and 19 cm focal length was used to project an image of the halogen lamp and its reflector onto the Taylor cone region. We used two nozzles of different diameter, which were placed 0.2 m (h) away from the collector. The inner and outer diameters of a small nozzle are 0.16 mm and 0.31 mm, resepctively, while those of a large nozzle are 0.838 mm and 1.2 mm. The polymeric solution used in the experiment was a mixture of of Poly-Methyl Methacrylate (PMMA) and DiMethyl Formamide (DMF) 10%wt.

A typical oscillatory behavior of jets taken at two different times is shown in Fig. 2. The small nozzle was used for the flow-rate of 0.4 ml/h and the electric charge of 5 KV. Initially the fluid travels downstream in axial direction (z-direction). As it moves further downstream, the bending instability plays a part causing the fiber to experience radial stretching while the axial velocity gradually decreases. From the picture, the ratio of the jet diamter (estimated near the nozzle tip) to the nozzle outer diameter is about 1:5. This means that the ratio of jet diamter to the nozzle inner diameter is 2:5. Then the diameter is further reduced during the evolution of liquid jet. The further reduction in diameter, which is measured at the end of loop in the picture, is abut 30%. This does not appear to be significant reduction, and will be further discussed in the theory section. It is interesting to note that the jet is not in parallel to its axis and bents to a radial direction due to some distaurbances. However the source is not identified yet.

The influence of an electrical potential difference, which is established between the surface of liquid drop and the collector, is shown in Fig. 3. The collector voltages used here are 5 KV and 10 KV, while other parameters are kept the same with the previous case. The bending instability occurs around the same location for both cases. For larger voltages, the radial stretching is relatively less significant and the jet diameter becomes smaller. This is because the attractive force from the collector increases with the increase of collector voltage.

The liquid jets for different flow rate and different nozzle inner diameter are compared and the results are shown in Fig. 4. For a large nozzle, the contact point between the fiber and the nozzle moves around at the tip of nozzle, and the excessive amount of fluid destabilizes the system by forming an oversized deposit at the nozzle tip when the applied voltage is relatively low. The increase of nozzle diameter does not affect much on the jet diameter, thus evolving profile is similar each other. From the pictures, the jet diamter estimated at the nozzle tip is about 0.08 mm for the small nozzle and 0.11 mm for the large nozzle. The bending instability in the tail of fiber is

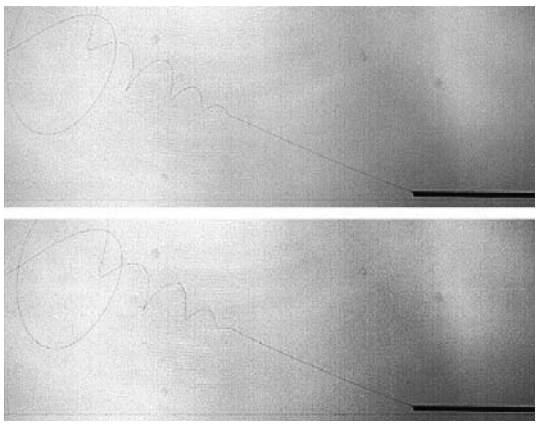

Fig. 2 Typical images of electrically driven liquid jets taken at different times. The inner diameter of the nozzle is 0.08 mm and the electric charge is 5 KV

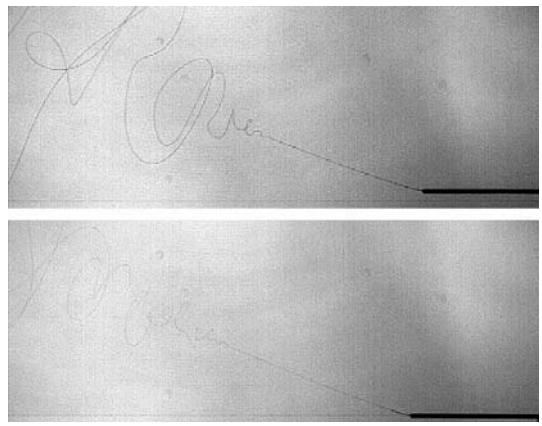

Fig. 3 The fiber responses to different voltages, 5 KV (above), 10 KV (below)

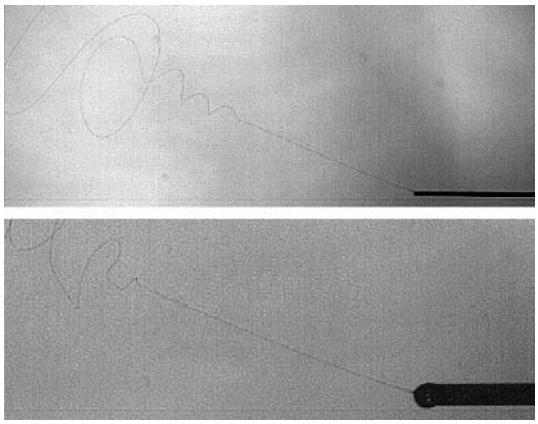

Fig. 4 The influence of flow rate and nozzle inner radius on the evolution of liquid jets, 0.4 ml/h and 0.08 mm (above), 0.08 ml/h and 0.419 mm (below)

pronounced a little bit for the smaller nozzle.

We have examined the influence of some parameters such as the collector voltage, flow-rate, and nozzle diameter. Our experiments reassured that the optimum values are required to produce nanofiber under various operational and geometrical conditions. For example, if the collector voltage is too big the radial stretching is suppressed by the axial elongation. The complex force balance will be further discussed by a mathematical model in the next section.

3. Viscoelastic Model

3.1 Viscoelastic dumbbell model for a jet segment

A linear viscoelastic model of Maxwell type is adopted for the charged flow of a liquid jet exiting from a nozzle, as shown in Fig. 5. First a segment of the jet is modelled as a spring and damper system, that is a viscoelastic dumbbell. Two successive beads, A and B, are assumed to preserve charge and mass denoted by e and m. The first bead, bead A, is fixed in the absence of the Coulomb force while bead B is under the influence of Coulomb force of repulsive nature $-e^2/l^2$, where l is the length of the segment. The force due to the external electrical field is given by $-V_0e/h$. A generalized Maxwellian

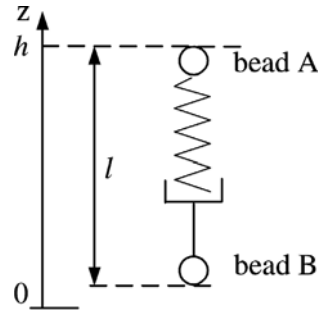

Fig. 5 A schematic view of a simple viscoelastic model

fluid obeys the following equation for the stress σ excited by the rate of deformation, dl/dt (Bird et al., 1987),

$$\frac{d\sigma}{dt}=G\frac{1}{l}\frac{dl}{dt}-\frac{G}{\mu}\sigma \tag{1}$$

where G is the elastic modulus, μ viscosity, and t time. It is well understood that the Maxwell model effectively represents the rheological behavior of concentrated polymeric fluid in excessive lateral deformation. The momentum balance for bead B is (Yarin 1993)

$$m\frac{dU}{dt}=-\frac{e^2}{l^2}-\frac{eV_o}{h}+\pi a^2\sigma \tag{2}$$

where a is the cross-sectional radius of the fluid segment and U is the velocity of bead B. The kinematic condition for the rate of deformation is related to the local bead velocity U by,

$$\frac{dl}{dt}=-U. \tag{3}$$

3.2 Nondiemnsional equations

We adopt the following non-dimensional parameters. l is nondimensionalized by L which is an initial segment length. t is divided by the relaxation time, $\theta=\mu/G$, which physically denotes the time required for a fluid to release accumulated stress. Stress σ is scaled by G, such that

$$\bar{l}=\frac{l}{L},\ \bar{a}=\frac{a}{L},\ \bar{t}=\frac{t}{\theta},\ \bar{\sigma}=\frac{\sigma}{G},\ \bar{U}=\frac{\theta U}{L} \tag{4}$$

Using the conservation of mass for a segment of initial radius of a_o at $t=0$,

$$\pi a^2 l=\pi a_o^2 L \tag{5}$$

the dimensionless form of Eqs. (1) ~ (3) becomes

$$\frac{d\bar{l}}{d\bar{t}}=-\bar{U}$$
$$\frac{d\bar{U}}{d\bar{t}}=F_{ve}\frac{\bar{\sigma}}{\bar{l}}-\bar{V}-\frac{Q}{\bar{l}^2} \quad (6)$$
$$\frac{d\bar{\sigma}}{d\bar{t}}=-\frac{\bar{U}}{\bar{l}}-\bar{\sigma}$$

where the dimensionless parameters are denoted by bars. Here three dimensionless parameters are,

$$Q=\frac{e^2\mu^2}{L^3mG^2},\ V=\frac{eV_o\mu^2}{hLmG^2},\ F_{ve}=\frac{\pi a_o^2\mu^2}{mLG} \quad (7)$$

Q represents the non-dimensional Coulomb force, V is electrostatic force in the presence of external electrical field, and F_{ve} represents the effect of inherent elasticity. If we choose the length scale as $L=(e^2/\pi a_oG)^{0.5}$, $Q\equiv F_{ve}$. However this is not restrictive and can be one of the important parameter to control the jet's dynamics. Note that the influences of evaporation and surface tension are neglected in the current model. The effect of solvent evaporation on the values of the rheological parameters of the polymer solution is not fully known at present.

3.3 Three-dimensional equations for the electrospun jets

With the analogy used in the previous section, we generalize a three-dimensional model system by a series of viscoelastic elements as shown in Fig. 6. Each bead has the charged amount e and the mass m. The length of the upper and the lower segment for bead i denoted by subscript u (up) and d (down), respectively are given by

$$l_{ui}=[(x_{i+1}-x_i)^2+(y_{i+1}-y_i)^2+(z_{i+1}-z_i)^2]^{0.5} \quad (8a)$$

$$l_{di}=[(x_i-x_{i-1})^2+(y_i-y_{i-1})^2+(z_i-z_{i-1})^2]^{0.5} \quad (8b)$$

where x, y and z are independent variables in Cartesian coordinate. The rates of strain of adjacent filaments are $(dl_{ui}/dt)/l_{ui}$ and $(dl_{di}/dt)/l_{di}$. The elastic forces acting on the upper and lower filaments of bead i are given in dimensional form,

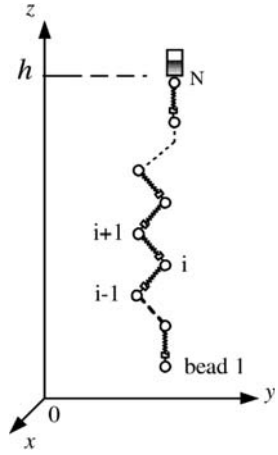

Fig. 6 A schematic view of a three-dimensional bead-spring model

$$\frac{d\sigma_{ui}}{dt}=G\frac{1}{l_{ui}}\frac{dl_{ui}}{dt}-\frac{G}{\mu}\sigma_{ui}$$
$$\frac{d\sigma_{di}}{dt}=G\frac{1}{l_{di}}\frac{dl_{di}}{dt}-\frac{G}{\mu}\sigma_{di} \quad (9)$$

The following conservation of mass is applied for the upper and lower filaments,

$$\pi a_{ul}^2 l_{ui}=\pi a_{di}^2 l_{di}=\pi a_o^2 L \quad (10)$$

For the 3-D model with the total number of beads N increasing over time, the net Coulomb force acting on the ith bead must be approximated by counting all the other beads existing in the system. The force balance is obtained for bead i from the second law of Newton. The right hand side of Eq. (11) consists of the Coulomb force, electrostatic force, viscoelastic force, and surface tension effect.

$$m\frac{d^2\mathbf{r}_i}{dt^2}=\sum_{j=1(j\neq i)}^{N}\frac{e^2}{R_{ij}^2}(\mathbf{r}_i-\mathbf{r}_j)-e\frac{V_o}{h}\mathbf{k}+\frac{\pi a_{ui}^2\sigma_{ui}}{l_{ui}}(\mathbf{r}_{i+1}-\mathbf{r}_i)$$
$$-\frac{\pi a_{di}^2\sigma_{di}}{l_{di}}(\mathbf{r}_i-\mathbf{r}_{i-1})-\frac{a\pi(a^2)_{ave}k_i}{(x_i^2+y_i^2)^{0.5}} \quad (11)$$
$$\times[\mathbf{i}|x_i|\mathrm{sign}(x_i)+\mathbf{j}|x_i|\mathrm{sign}(x_i)]$$

where $\mathbf{r}_i$ is a position vector for bead i, which has three components (x, y and z). a is the surface tension coefficient, k_i is the local curvature, and $a_{av}=(a_u+a_d)/2$. The symbol sign(x) is a unit vector, providing the direction of surface tension force. If $x>0$ $(x<0)$ then, sign$(x)=$

$1(=-1)$, while $\text{sign}(x)=0$ when $x=0$. R_{ij} denotes the distance from bead i to bead j, and solely depends on the geometry of beads.

$$R_{ij}=[(x_i-x_j)^2+(y_i-y_j)^2+(z_i-z_j)^2]^{0.5} \quad (12)$$

Upon adopting the scaling factors and parameters introduced in Eqs. (4) and (7), together with additional non-dimensional parameters,

$$A=\frac{a\pi a_o^2\mu^2}{mL^2G^2},\ K_s=\frac{\omega\mu}{G},\ H=\frac{h}{L} \quad (13)$$

the momentum conservation results in three components in dimensionless form,

$$\frac{du_i}{dt}=Q\sum_{j=1(i\neq j)}^{N}\frac{(x_i-x_j)}{R_{ij}^3}+F_{ve}\left[\sigma_{ui}\frac{(x_{i+1}-x_i)}{l_{ui}^2}-\sigma_{di}\frac{(x_i-x_{i-1})}{l_{di}^2}\right]-A\frac{(a_{ui}+a_{di})^2k_ix_i\text{sign}(x_i)}{4\sqrt{x_i^2+y_i^2}} \quad (14a)$$

$$\frac{dv_i}{dt}=Q\sum_{j=1(i\neq j)}^{N}\frac{(y_i-y_j)}{R_{ij}^3}+F_{ve}\left[\sigma_{ui}\frac{(y_{i+1}-y_i)}{l_{ui}^2}-\sigma_{di}\frac{(y_i-y_{i-1})}{l_{di}^2}\right]-A\frac{(a_{ui}+a_{di})^2k_iy_i\text{sign}(y_i)}{4\sqrt{x_i^2+y_i^2}} \quad (14b)$$

$$\frac{dw_i}{dt}=Q\sum_{j=1(i\neq j)}^{N}\frac{(z_i-z_j)}{R_{ij}^3}+F_{ve}\left[\sigma_{ui}\frac{(z_{i+1}-z_i)}{l_{ui}^2}-\sigma_{di}\frac{(z_i-z_{i-1})}{l_{di}^2}\right]-V \quad (14c)$$

Note that the upper bar notation is eliminated for simplicity in Eq. (14) and the preceding equations. Then the dimentionless form of the stress is,

$$\frac{d\sigma_{di}}{dt}=\frac{1}{l_{di}}\frac{dl_{di}}{dt}-\sigma_{di},\ \frac{d\sigma_{ui}}{dt}=\frac{1}{l_{ui}}\frac{dl_{ui}}{dt}-\sigma_{ui} \quad (15)$$

A coupled system of Eqs. (10), (14) and (15) are solved using numerical integration for every beads at every time step. Upon inception at $t=0$, the stress components, σ_{ui} and σ_{di}, as well as the local velocity are assumed to zero.

The initial number of bead (N) is given by 2. When N increases, the first bead is pushed downstream till it reaches the collector. Once any bead reaches the collector, it is removed from calculation. The generation of new bead (nth) always occurs at the nozzle exit. If the distance between this bead and the nozzle tip exceeds a certain criteria, a new bead is added. Finally a time dependent sinusoidal perturbation with frequency ω is used for every new bead inserted.

$$x_i/L=10^{-3}\sin(\omega t)$$
$$y_i/L=10^{-3}\cos(\omega t) \quad (16)$$

3.4 Results

In this section we present the theoretical predictions for the jet paths calculated from the electrically driven bending instability. The positions of all beads N are calculated at every time step. The required parameters are density, viscosity, surface tension coefficient and bulk modulus. Some reference values are taken from the similar polymeric blend used by Reneket et al. (2000). The carried charge by the jet was estimated to be 1 C/l (Yarin 1993), which is the value we used in our simulation as well. More realistic parameters are obtained from our experiments.

For the first analysis, the adopted properties are $a_0=150$ μm, $\rho=10^3$ Kg/m^3, $h=2$ m, $V_0=10$ KV, $\alpha=0.07$ Kg/s^2, $\mu=10^3$ Kg/ms, $G=10^5$ Kg/ms^2. The corresponding non-dimensional parameters are $Q=F_{ve}=78356$, $V=156.8$, $A=17.21$, $H=627.3$, $K_s=100$. The charge on each bead is $e=2.68\times10^{-4}$ kg$^{1/2}$m$^{3/2}$/s$=2.83\times10^{-9}$ C. The mass of a bead is $m=2.83\times10^{-9}$ Kg. The relaxation time $\theta=\mu/G=0.01$, which is equivalent to the typical lab noise range of $\omega=10^4$/s. Q and F_{ve} are often of the same order of magnitude each other while the non-dimensional surface tension coefficient (A) is relatively small. Figure 7 illustrates the predicted development of typical jet paths estimated at different time steps. There is virtually no difference between $t=0.8$ and $t=1.0$ in the figure, indicating that the fiber profile is fully developed. The evolution of fiber exhibits the similar response as it was shown in the experiment. It can be noted that in the experiment only the region near the vertex of the envelope cone was imaged in order to capture the development of instability in detail. This is because the liquid jet is very thin. The influences of gravity,

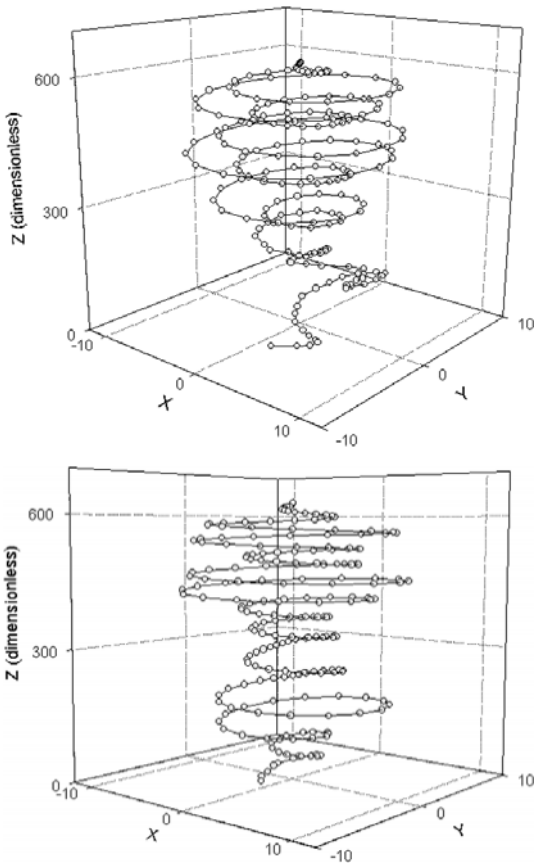

Fig. 7 The fully-developed profile of charged jets at two different times, $\bar{t}=0.8$ and $\bar{t}=1.0$

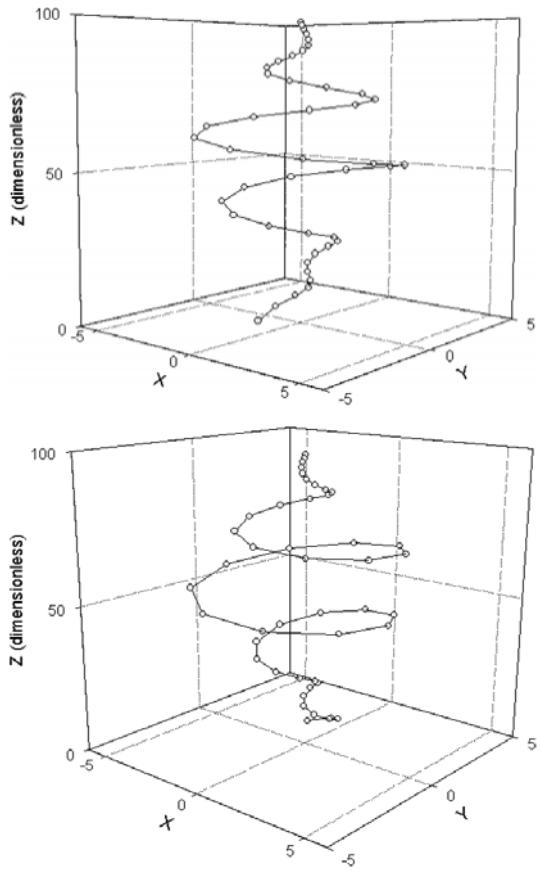

Fig. 8 Charged jets with values of the dimensionless parameters, $Q=F_{ve}=14683$, $V=176$, $A=1.36$, $K_s=80$, $H=99.2$, at two different time $\bar{t}=0.5$ and $\bar{t}=1.0$

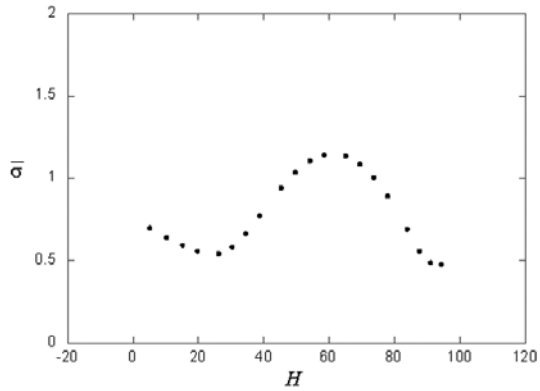

Fig. 9 Longitudinal stress along the jet with values of the dimensionless parameters in Fig. 8

surface tension, and evaporation can be negligible, although the surface tension is taken into account.

Consider now the development of perturbations into a bending instability in a realistic jet, which is quite similar with the current experiment. The adopted properties are $a_0=100$ μm, $\rho=10^3$ Kg/m^3, $h=0.2$ m, $V_0=5$ KV, $\alpha=0.07$ Kg/s^2, $\mu=10^3$ Kg/ms, $G=2\times10^5$ Kg/ms^2. The corresponding non-dimensional parameters are $Q=F_{ve}=16416.8$, $V=123.2$, $A=1.7$, $H=88.7$, $K_s=100$. The charge and the mass of a bead is assumed to be the same with the previous case. Figure 8 shows the predited jet paths estimated at two different time steps, which indicate the fully developed pofiles. The most efficient stretching occurs almost in the middle of fiber and levels off at the tail of fiber, which was also observed in the previous experiments. If more beads are generated, the stretching continues until the elas-

tic force due to deformation overcomes the Coulomb force. The result in Fig. 9 shows the distribution of the logitudinal stress along the jet. The maximum appears before the middle of the jet.

4. Conclusions

A combined experimetnal and theoretical study has been conducted to analyze the evolution of an electrically driven liquid jet of polymer solutions. The study indicates that the profile of fiber jets is governed by the parameters such as the distance between the nozzle and collector, the charge voltage, material properties, and the nozzle radius. The experimental data of the jet paths captured by high-speed videocamera has successfully captured the unsteady bending instability. A viscoelastic rheological model, which takes the competing force components such as the Coulomb force, electrostatic force, viscoelastic force, and surface tension effects into account, has confirmed the similar results observed in the experiments. The theory using the best values for rheological and electrial parameters of the polymer solutions can predict the general behavior of the liquid jets. However, the following assumption and definition made in the model requires further investigations; (1) the ionic charge is fixed in the fluid and moves with the jet, (2) using the definition of length scale L as an initial segment length such that $Q=F_{ve}$. This is because L controls the total number of beads N existing in the system, and N also governs the evolution of the electrically driven liquid jets.

Acknowledgments

This work was supported by grant No. (R01-2003-000-10072-0) from the Basic Research Program of the Korea Science & Engineering Foundation.

References

Baumgarten, P. K., 1971, "Electrostatic Spinning of Acrylic Microfibers," *Journal of Colloid Interface Science*, Vol. 36, pp. 71~79.

Bird, R. B., Armstrong, R. C. and Hassager, O., 1987, *Dynamics of Polymeric Liquids*, 2nd ed., Wiley, New York.

Dersch, R., Liu, T., Schaper, A., Greiner, A. and Wendorff, J., 2003, "Electrospun Nanofibers: Internal Structure and Intrinsic Orientation," *Journal of Polymer Science Part A: Polymer Chemistry*, Vol. 41, pp. 545~553.

Doshi, J. and Reneker, D. H., 1995, "Electrospinning Process and Application of Electrospun Fibers," *Journal of Electrostatics*, Vol. 35, pp. 151~160.

Fang, X. and Reneker, D., 1997, "DNA Fibers by Electrospinning," *Journal of Macromolecular Science, Part B: Physics*, Vol. 36, pp. 169~173.

Formhals, A., 1934, "Process and Apparatus for Preparing Artificial," U. S. Paten 1, 975, 504.

Horning, D. and Hendricks, C., 1979, "Study of an Electically Driven Jet," *Journal of Applied Physics*, Vol. 50, No. 4, pp. 2614~2617.

Larrondo, L. and Manley, J. R. St., 1981, "Electrostatic Fiber Spinning from Polymer Melts. III. Electrostatic Deformation of a Pendant Drop of Polymer Melt," *Journal of Polymer Science*, Vol. 19, pp. 933~940.

Pedicini, A. and Farris, R., 2003, "Mechanical Behavior of Electrospun Polyurethane," *Polymer*, Vol. 44, pp. 6857~6862.

Rayleigh, Lord, 1882, "On the Equilibrium of Liquid Conducting Masses Charged with Electricity," *Philos. Mag.*, Vol. 44, pp. 184~186.

Reneker, D. and Chun, I., 1996, "Nanometer Diameter Fibres of Polymer Produced by Electrospinning," *Nanotechnology*, Vol. 7, pp. 216~223.

Reneker, D., Yarin, A., Fong, H. and Koomhongse, S., 2000, "Bending Instability of Electrically Charged Liquid Jets of Polymer Solutions in Electrospinning," *Journal of Applied Physics*, Vol. 87, No. 9, pp. 4531~4547.

Shin, Y. M., Hohman, M. M., Brenner, M. P. and Rutledge, G. C., 2001, "Electrospinning: A Whipping Fluid Jet Generates Submicron Polymer Fibers," *Applied Physics Letter*, Vol. 78 No. 8, pp. 1149~1151.

Taylor, G., 1964, "Disintegration of Water

Drops in an Electric Field," *Proceedings of the Royal Society of London, Series A, Mathematical and Physical Sciences*, Vol. 280, No. 1382, pp. 383～397.

Viswanathamiruthi, P., Bhattarai, N., Kim, H., Lee, D., Kim, S. and Morris, M., 2003, "Preparation and Morphology of Niobium Oxide Fibres by Electrospinning," *Chemical Physics Letters*, Vol. 374, pp. 79～84.

Yarin, A. L., 1993, *Free Liquid Jets and Films : Hydrodynamics and Rheology*, Longman, Harlow and Wiley, New York.